We are IntechOpen, the world's leading publisher of Open Access books Built by scientists, for scientists

4,800
Open access books available

122,000
International authors and editors

135M
Downloads

Our authors are among the

154
Countries delivered to

TOP 1%
most cited scientists

12.2%
Contributors from top 500 universities

CLARIVATE ANALYTICS BOOK CITATION INDEX INDEXED

WEB OF SCIENCE™

Selection of our books indexed in the Book Citation Index in Web of Science™ Core Collection (BKCI)

Interested in publishing with us?
Contact book.department@intechopen.com

Numbers displayed above are based on latest data collected.
For more information visit www.intechopen.com

17

Fiber Optic Temperature Sensors

S. W. Harun[1,2], M. Yasin[1,3], H. A. Rahman[1,2,4], H. Arof[2] and H. Ahmad[1]
[1]*Photonic Research Center, University of Malaya, Kuala Lumpur*
[2]*Department of Electrical Engineering, University of Malaya, Kuala Lumpur*
[3]*Department of Physics, Faculty of Science and Technology, Airlangga University, Surabaya*
[4]*Faculty of Electrical Engineering, Universiti Teknologi MARA (UiTM), Shah Alam*
[1,2,4]*Malaysia*
[3]*Indonesia*

1. Introduction

The need for temperature measurement exists in many applications such as in automated consumer products, automated production plants and high performance processors. Recent works have mainly focused on temperature sensors that satisfy user requirements for specific applications, and the main considerations are performance, dimension and reliability. In fact, traditional low-cost solutions, such as thermocouples and resistance temperature detectors (RTDs), do not always yield satisfactory performance, e.g., when the fluid temperature has to be measured in hostile environments, in the presence of electromagnetic, chemical, and mechanical disturbances. Since signals from the thermoelectric sensors are normally mixed with intrinsic noise and extrinsic interferences, they may contain intolerable errors if not properly filtered. Therefore, this type of sensors is inept for gauging temperature in microfluidic or nano-sized devices, in extreme marine environments, and underground geological sites where long distance measurement with precision is required. For such applications, fiber optical sensors offer a better alternative since the optical signal does not suffer from interference by electromagnetic fields and can be transmitted over extremely long distances without any significant loss [Yasin et al., 2010; Li et al., 2010; Ahmad et al., 2009; Lim et al., 2009; Ahmad et al., 2009; You et al., 2005; Xu et al., 2005]. Furthermore, they are relatively small in size, and compatible with other optical fiber devices.

To date, various types of fiber optic temperature sensors have been reported in the literatures and they are mostly based on fiber interferometric [Choi et al., 2008] and fiber Bragg grating (FBG) [Han et al., 2004]. However, the first type of sensors are rather expensive to produce and complicated to implement on-site [Golnabi, 2000]. Fiber Bragg gratings are very efficient at temperature sensing and are easy to implement; however, they always need additional techniques to discriminate the Bragg shifts by temperature and by strain/compression and they also require expensive phase-masks. In this chapter, a temperature sensor is demonstrated based on four different techniques; intensity modulated

fiber optic displacement sensor (FODS), lifetime measurements, microfiber loop resonator (MLR) and stimulated brillouin scattering. The first sensor is based on a rugged, low cost and very efficient FODS utilizing a plastic optical fiber (POF)-based coupler as a probe and a linear thermal expansion of aluminum. The second temperature sensor, which is based on fluorescence decay time in Erbium-doped silica fiber has the advantage of incorporating a time based encoding system, which is less sensitive to system losses such as those associated with optical cables and connectors. The MLR is formed by coiling a microfiber, which was obtained by heating and stretching a piece of standard silica single-mode fiber (SMF). The MLR is embedded in a low refractive index material for use in temperature measurement. The MLR-based temperature sensor has a low loss splicing with a standard SMF. Lastly, a temperature sensor is demonstrated using an SBS effect, which requires measurement of frequency shift. In the proposed sensor, a Brillouin pump is injected into one end of a ring cavity resonator, in which a sensing fiber is located, and then the frequency shift between the BP and the Brillouin fiber laser (BFL) output is measured using a heterodyne method.

2. FODS based temperature sensing

POFs have widespread uses in the transmission and processing of optical signals for optical fiber communication system compatible with the Internet. POFs also have potential applications in WDM systems, power splitters and couplers, amplifiers, sensors, scramblers, integrated optical devices, frequency up-conversion, and etc. [Yasin et al., 2009; Yang et al., 2011]. Recently, an intensity modulated FODSs have been demonstrated to be efficient for many applications including sensor. They are relatively inexpensive, easy to fabricate and suitable for deployment in harsh environments. In this section, a low cost temperature sensor is demonstrated using POF-based coupler as a probe based on a linear thermal expansion of aluminum. The temperature sensor is schematically shown in Fig. 1. The sensor is essentially a FODS with a 3 dB multimode fiber coupler as a probe. A 594 nm He-Ne beam is launched into port 1 of the coupler. Light travels to port 3 and is scattered when it exits the fiber end. It is then reflected by the top surface of an aluminium rod with dimensions of 0.5 cm diameter and 7 cm length. The port 3 probe is held in position about 1 mm perpendicular to the top surface of the aluminium rod so that the reflected light can be easily launched back into the same port. The collected light is sent to port 2 by the 3dB coupler and measured by a silicon photo-detector. The detector converts the light into electrical signal, which is then processed by the lock-in amplifier and finally displayed and stored onto the computer.

In the calibration stage, the static operating range of the probe is identified and this process requires the probe to be mounted on a translational stage, which is rigidly attached to a vibration free table. Firstly, the output from port 2 at zero point is measured, where the aluminum rod and the probe are in close contact. Then the aluminum rod is moved away from the probe in 50 μm steps and at each position, under vibrationless condition, the output voltage is recorded. A graph of displacement (gap) against output voltage is drawn and a linear range on the graph is identified. A position at the center of the linear range is chosen and the gap between the probe and the top surface of the aluminum rod is fixed at the chosen displacement point. Then an experiment is carried out where the aluminum is fixed onto a hotplate for heating purpose. A thermocouple placed at the upper region of the aluminum rod is used to display and monitor the temperature of the aluminum rod. The

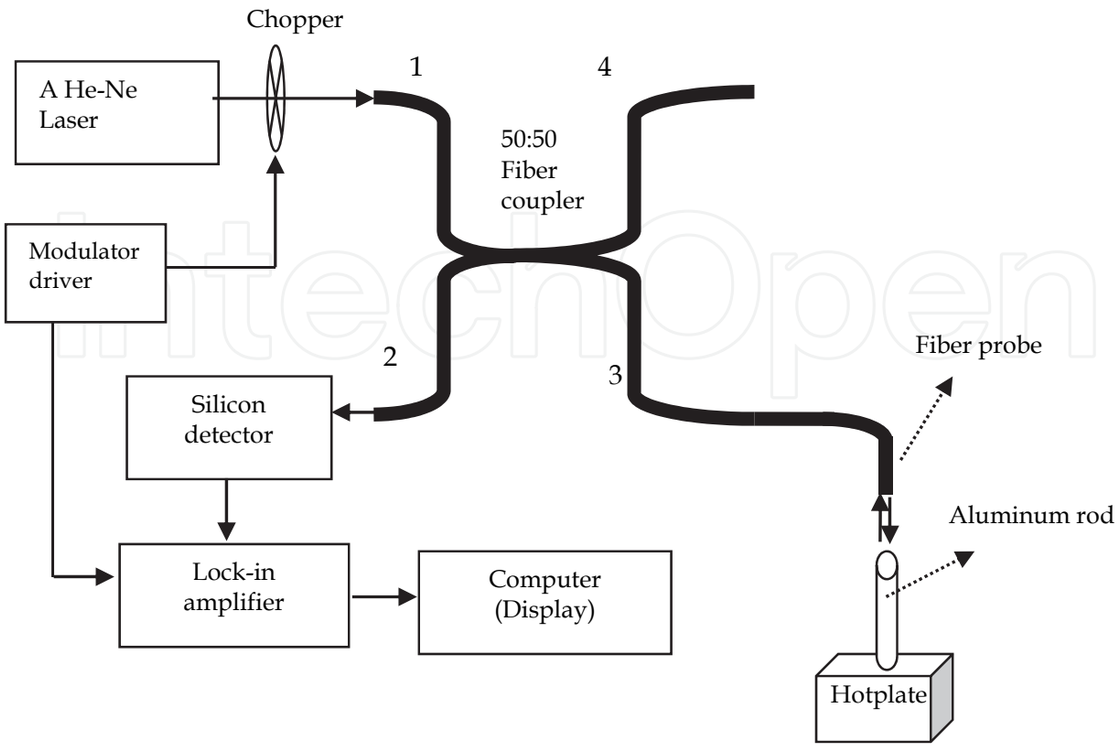

Fig. 1. Experimental setup for the proposed temperature sensor using a POF-based coupler

thermocouple has a resolution of 10C and a temperature range of -500C to 13000C. The heat to the aluminum rod is controlled by varying the heat intensity produced by the hotplate ranging from room temperature (250C) to 900C.

Fig. 2 show the efficiency of the FODS as a function of displacement obtained both experimentally and theoretically without the temperature effect. The characteristic of the proposed sensor can be compared with the case of coupling two similar collinear fibers which are separated at the end-faces and with both axis aligned as discussed in [Yang et al., 2011]. Given that the the distance between the parallel end-faces is called z, a and NA is the radius and numerical aperture of the fiber respectively, the efficiency η for small values of z/a is [Van Etten, 1991]

$$\eta = 1 - \frac{z}{a}\frac{2}{\pi(NA)^2}\left[arcsin(NA) - NA\sqrt{1-NA^2}\right] \quad (1)$$

for z/a <<1

The fiber receives the maximum light when the gap between the tip of fiber probe and the reflected surface is zero, and thus the measured intensity of the reflected light is maxima as shown in the figure. However, the measured intensity of the reflected light decreases almost linearly as the distance or gap increases especially for close distance target. Theoretically, the distance and the reflected power vary according to the inverse square law and the ratio between the reflected power and the transmitted power is given by [Kulkarini et al., 2006]

$$\frac{P_r}{P_t} = \frac{d^2}{(2x\tan\theta)^2} \tag{2}$$

where Pr, Pt, d, x, and θ are the reflected power, transmitted power, core diameter, axial displacement and fiber's acceptance angle, respectively. The characteristic of the displacement curve is summarized in Table 1 where the sensitivity is obtained at 0.0005 mV/μm and the slope shows a good linearity of more than 99% within the displacement range of 1400 μm. The displacement sensor is observed to be very stable with the measurement error of less than 0.8%.

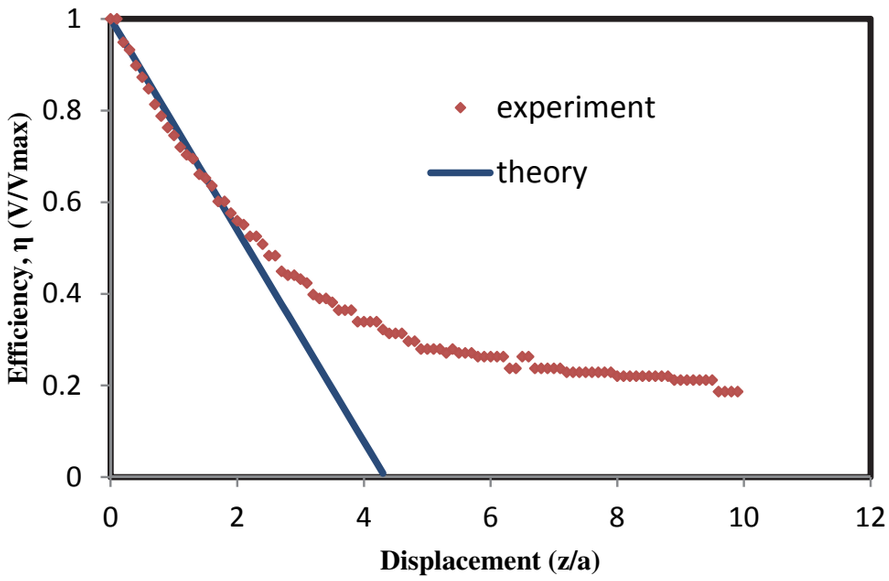

Fig. 2. Efficiency as a function of displacement obtained both experimentally and theoretically.

Parameter	Value
Sensitivity	0.0005 mV/μm
Linear Range	0 – 1400 μm
Linearity	More than 99%
Standard Deviation	0.01 mV (0.8%)
Resolution	19 μm

Table 1. The Performance of fiber optic displacement sensor using the aluminum rod.

Fig. 3 show the linear function of the output signal against the aluminum rod temperature for two different runs. The two different runs were taken because repeatability of results is a crucial factor in the operation of any sensor system. In the experiment, the gap between the aluminum rod and fiber tip of port 3 is fixed at 1 mm, which is within the linear range of the displacement response without the temperature effect. The temperature of the aluminum rod is then varied from 250C to 900C, resulting in an output signal ranging from 0.95 mV to

1.20 mV. The output signal starts to significantly increase with increasing rod temperature at 420C, which henceforward forms a linear function until the rod temperature reaches 900C. It is observed that the maximum difference between the two runs is about 0.04 mV, which is small compared to the full range of 1.20 mV. The temperature sensor is observed to be very stable with the measurement error of less than 0.8% which is obtained at 900C (see inset of Fig. 3). The output voltage are recorded for 200 seconds and the standard deviation obtained at 250C, 600C and 900C are 0.5%, 0.5% and 0.8% respectively. The performance of the temperature sensor is summarized in Table 2 where the sensitivity of the linear function for the first run is 0.0044 mV/0C with 98% linearity whereas the sensitivity of the linear function for the second run is 0.0041 mV/0C with 96% linearity.

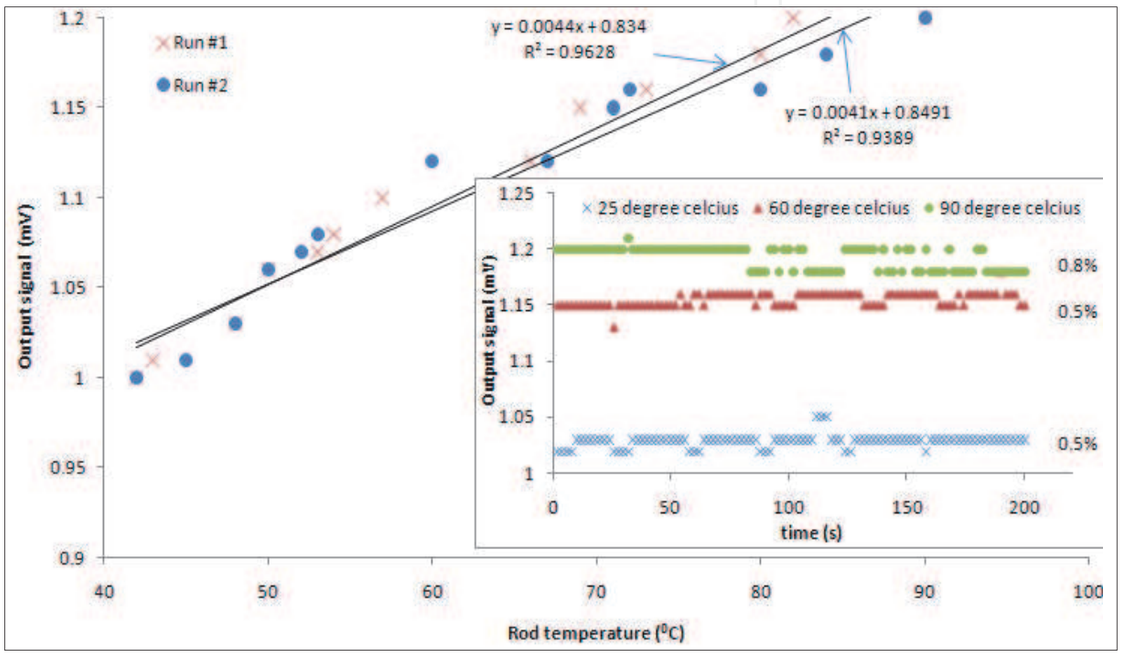

Fig. 3. Linear relationship between the output voltage and aluminum rod temperature for 25⁰C to 90⁰C. Inset shows the standard deviation values for output voltage versus rod temperature at 25⁰C, 60⁰C and 90⁰C.

Parameter	Value (Run No. 1)	Value (Run No. 2)
Sensitivity	0.0044 mV/°C	0.0041 mV/°C
Linear Range	42 - 90 °C	42 - 90 °C
Linearity	More than 98%	More than 96%
Standard Deviation	± 0.01 mV	± 0.01 mV
Resolution	2.4 °C	2.4 °C

Table 2. The performance of the temperature sensor using FODS.

The temperature sensor has a higher sensitivity (0.0044 mV/0C) compared to the displacement sensor (0.0005 mV/μm) even though the initial gap between the aluminum rod and fiber tip of port 3 is fixed at 1 mm, which is within the linear range of the displacement response without temperature effect. This is because as temperature increase,

the reflectivity of aluminum will also increase [Guo et al., 2003], hence sensitivity increases when increasing temperature is applied to the aluminum rod. The possible sources of error in the sensor operation can be due to light source fluctuation, stray light and possible mechanical vibrations. To reduce these effects a well-regulated power supply is used for the 594 nm He-Ne laser and this minimizes the fluctuation of source intensity. The sensor fixture is also designed so that the stray light cannot interfere with the source light and room light does not have any effect on the output voltage. To reduce the mechanical vibrations, the experimental set-up is arranged on a vibration free table

3. Fiber optic temperature sensor based on lifetime measurement

Fluorescence-based sensors are widely used for measuring various parameters due to its relatively independent of ambient conditions. This approach is widely used for temperature sensor, which is normally based on the detection of fluorescence lifetimes in various rare-earth-doped silica fibers [Zhang et al., 2009; Lopez et al., 2004; Seat et al., 2002; Baek et al., 2006]. In principle, fluorescence is induced by pump power at a certain wavelength that is suitable for the doped ions, and only a straightforward detection procedure is needed. An additional advantage of such rare-earth-doped fiber sensors is that they are compatible with a wide range of existing fiber-optic multiplexing schemes that can simultaneously detect multiple physical parameters. The underlying principle behind the ability of the rare-earth doped materials to be used as temperature sensors [McSherry et al., 2005] is their properties of emission and absorption that are dependent on the temperature. This behavior is due to the homogeneous broadening of the line width and the changing population of the energy levels with temperature. In the earlier work, a remote temperature sensor has been proposed using fluorescence intensity-ratio technique [Castrellon-Uribe, 2005]. In this section, a temperature sensor is proposed based on fluorescence decay time in Erbium-doped fiber (EDF).

Fig. 4 shows the schematic diagram of the proposed sensor set-up. The 980nm laser pump beam is launched into a piece of 90 cm long Erbium-doped fiber (EDF) via a wavelength division multiplexing (WDM) coupler. The EDF is placed in a vacuum oven which allows us to vary the fiber temperature within 25 to 200oC interval. The fluorescence signal from the forward pumped EDF is detected by a Ge photo-detector and processed with a digital oscilloscope. The 980 nm pump beam is chopped so as to generate a square-wave modulated signal with pulse width of 2.2ms, peak power of approximately 124mW and frequency of 45Hz. When the erbium-doped fiber is pumped with the photon energy of 980 nm, the $^4I_{11/2}$ erbium level is excited and the $^4I_{13/2}$ metastable level is quasi-instantaneously populated due to the non-radiative transition. The population inversion between $^4I_{13/2}$ and $^4I_{11/2}$ level is responsible for the emission of fluorescence at around 1550 nm. When the EDF is pumped at a fixed rate, the fluorescence variation including a lifetime change can reflect corresponding temperature. The temperature dependent fluorescence lifetimes of the spontaneous emission of the EDF is investigated and studied in this work.Fig. 5 shows the output spectrum of the amplified spontaneous emission (ASE) of the forward pumped EDF when the continuous wave pump power is fixed at 31 mW. The ASE spectrum peaks at 1529 nm with the average power of around -58 dBm. The temperature sensing mechanism in this work is based on the temperature dependence of the Erbium fluorescent lifetime decay. The Erbium fluorescence lifetime is measured using a modulated pump laser with power of

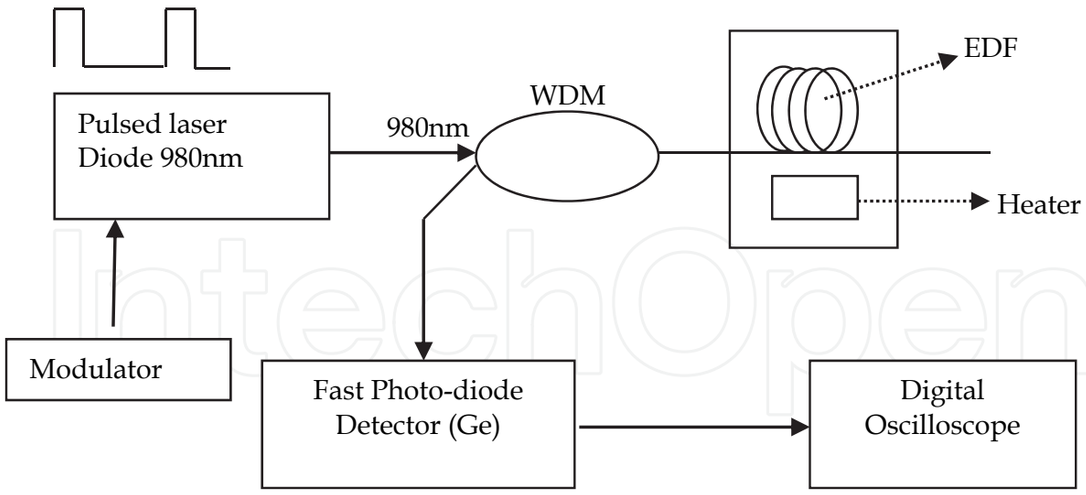

Fig. 4. Experiment setup of fiber optic high temperature sensor.

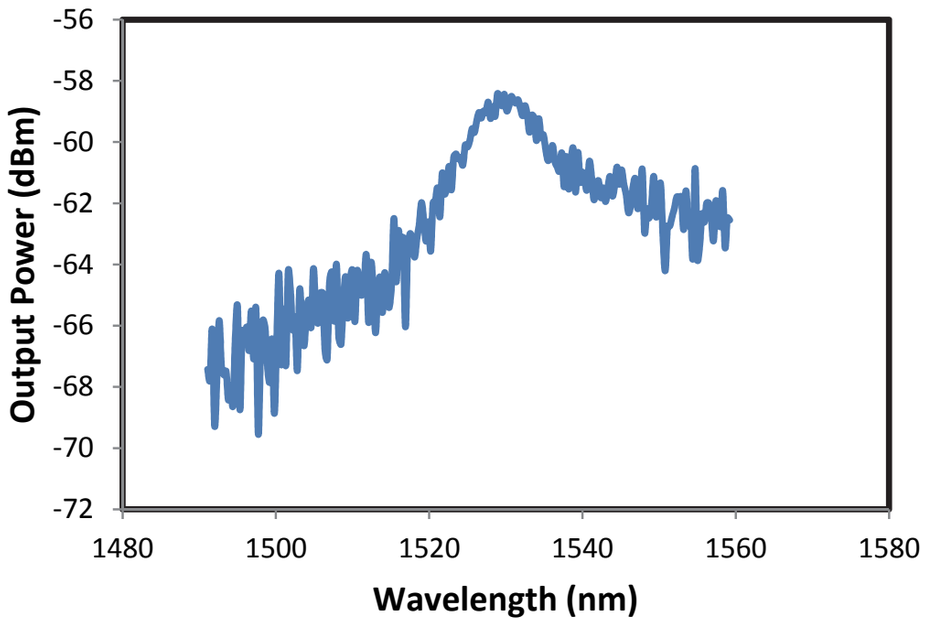

Fig. 5. Output spectrum of the generated ASE with 980nm pump power of 31mW.

approximately 2 mW and the results for temperature measurements of 85°C and 130°C are shown in Figs. 6(a) and (b), respectively. Fitting the exponential curve produces lifetimes of 4.85 and 4.75 ms for temperatures of 85°C and 130°C accordingly. The fluorescence lifetime data taken over the range of 25°C to 160°C are presented in Fig. 7. The graph shows the existence of an inverse linear relationship between the Erbium lifetime and the temperature. The fluorescence lifetime data shown in Fig. 7 are mean values of consecutive measurements at corresponding stabilized temperature. The sensitivity of the sensor is obtained at 0.009 ms/°C with a linearity more than 94%. The lifetime reduction is attributed to the quenching of the Erbium luminescence, which results in less efficient excitation. The quenching is mainly due to a decrease in the absorption coefficient of Erbium ion as the temperature is increased.

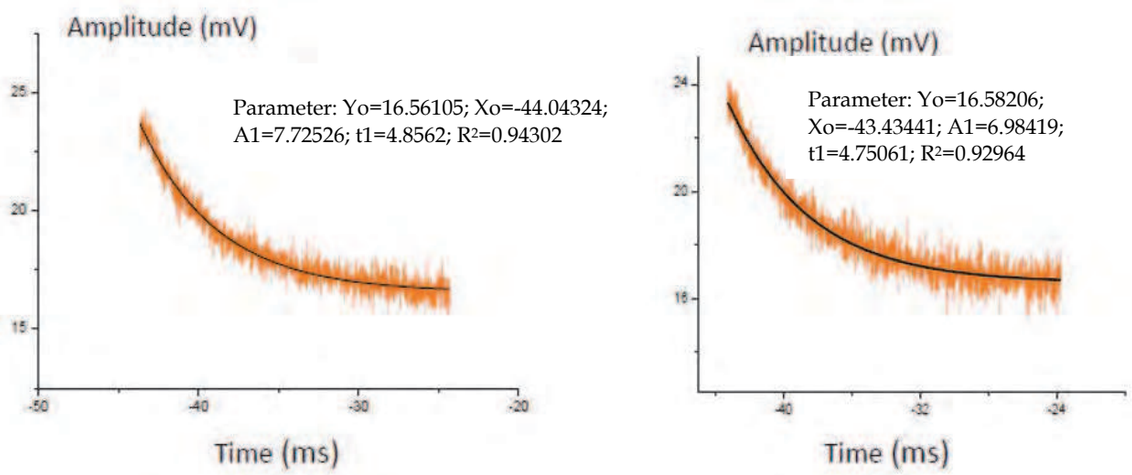

(a) 85 °C (b) 130 °C

Fig. 6. Fluorescence lifetime decay of EDF at (a) 85 °C and (b) 130 °C from a digital oscilloscope.

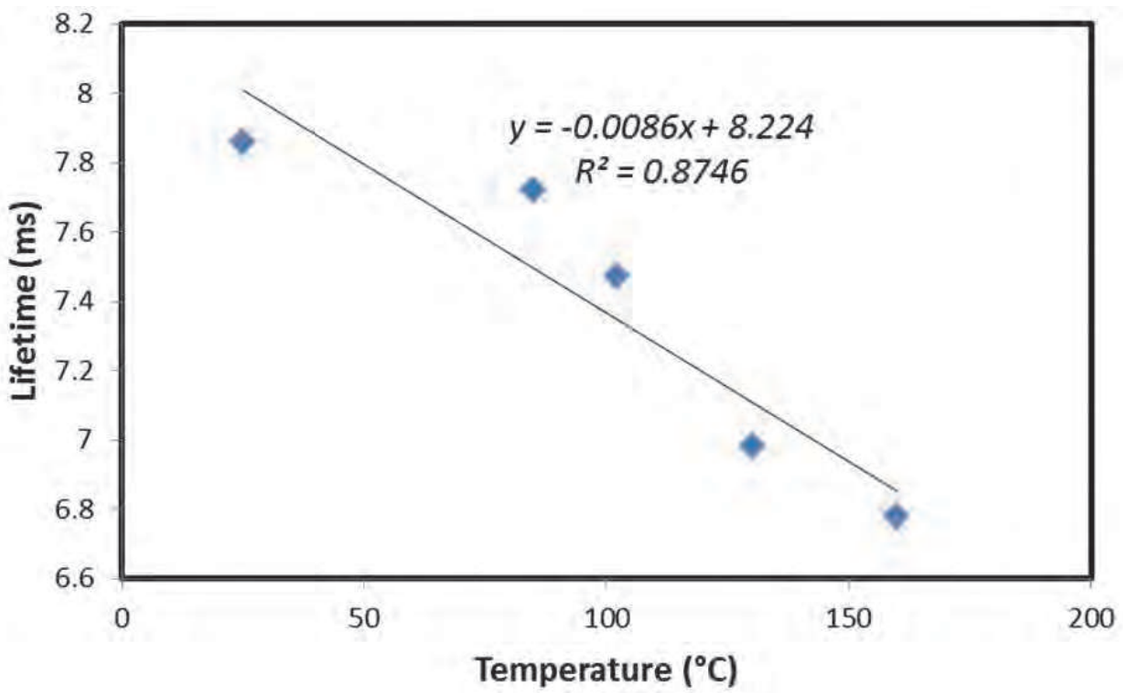

Fig. 7. Lifetime of EDF as function of Temperature.

4. Microfiber loop resonator based temperature sensor

Optical ring resonators have attracted considerable attention owing to their simple structure, compact size, and many applications in communication, optical signal processing and optical devices [Amarnath et al., 2005; Harun et al., 2010]. Planar waveguide micro-ring resonators have been well developed, but suffer from larger connection-losses with fibers and higher cost. Recently, research on low-loss microfibers has opened up new

opportunities for developing micro-photonic devices such as resonators [Jiang et al., 2006], couplers [Tong et al., 2006], and sensors [Li & Tong, 2006]. As one of the basic functional elements, microfiber resonators, in forms of loops, knots, or coils, have shown high intrinsic optical quality and have exhibited promising applications such as filters and lasers [Jiang et al., 2006]. Microfiber-based sensors are amongst the simplest of such devices, as they do not require expensive and complex fabrication procedures. Recently, strain, high temperature and refractive index sensing using tapered micro-structured optical fiber has been reported [Nguyen et al., 2005; Minkovich et al., 2005; Villatoro et al., 2006]. However, the authors used tapered micro-structured fiber which is expensive and difficult to work with in term of getting low loss splicing with standard optical fiber.

A microfiber fabrication set-up is shown in Fig. 8. A coating removed standard SMF was held by two fiber holders which were fixed on two translation stages. One stage is fixed and another stage is a motorized stage that can be moved in one dimensional direction and the speed of the motor can be controlled. The fiber ends were connected to an amplified spontaneous emission (ASE) source and an optical spectrum analyzer (OSA). The microfiber was fabricated by heating the fiber to its softening temperature, and then pulling the ends apart to reduce the fiber's diameter down to a around 1-3 mm. A high temperature and stable micro-burner fueled by clean butane gas is used in the tapering. Mounted on the movable stand, the micro-burner can be swung vertically to flame brush the tapered fiber. The flame should be clean and the burning gas flow should be controlled carefully so that the air convection does not break the fiber during the drawing process. During the tapering process, we monitored both the inter-modal interference and the insertion loss of the fiber using the ASE source in conjunction with the OSA. The flame is applied to the fiber in an optimized angle to make sure the heat distribution is homogeneous.

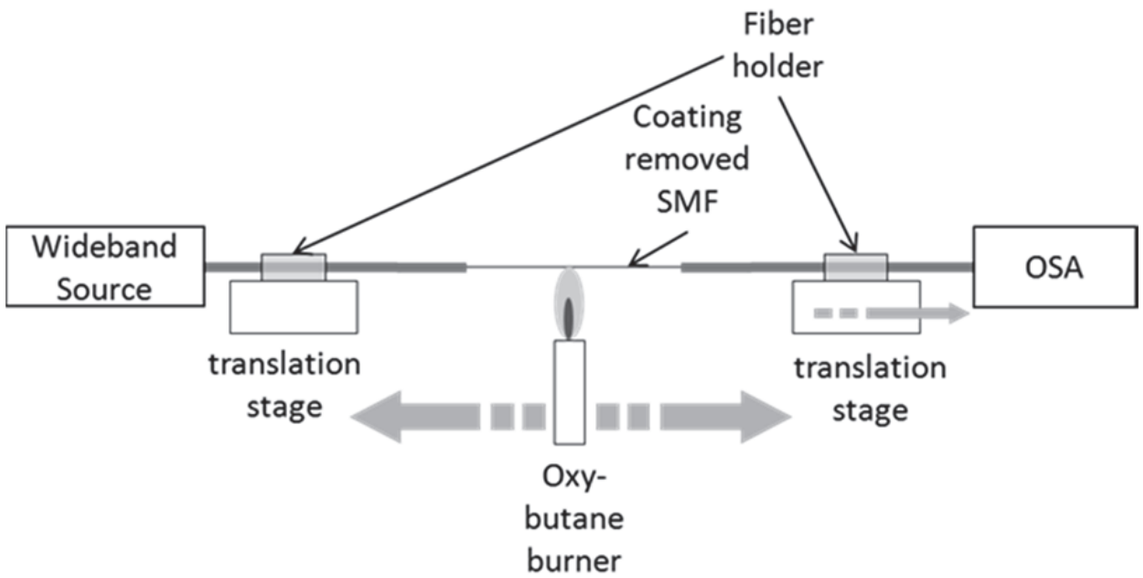

Fig. 8. Schematic diagram of the microfiber fabrication set-up.

The MLR is fabricated by coiling the microfiber onto itself using two surface attractions, van der Waals force and electrostatic force, which keep the loop stable since the forces overcome the elastic force to make the fiber straight. The fabricated MLR is laid on an earlier prepared

glass plate with a thin and flat layer of low refractive index material to address the temporal stability of the device as shown in Fig. 9. The thickness of the low refractive index material is approximately 0.5mm which is thick enough to prevent leakage of optical power from the microfiber to the glass plate. Some uncured resin is also applied on surrounding the MLR before it is sandwiched by another glass plate with the same low refractive index resin layer from the top. It is essentially important to ensure that minimum air bubbles and impurity are trapped around the fiber area between the two plates. This is to prevent refractive index non-uniformity in the surrounding of microfiber that may introduce loss to the system. The uncured resin is solidified by the UV light exposure for 3 ~7 minutes and the optical properties of the MLR are stabilized. The packaged MLR is located in an oven with temperature control to investigate how the comb spectrum changes with the temperature.

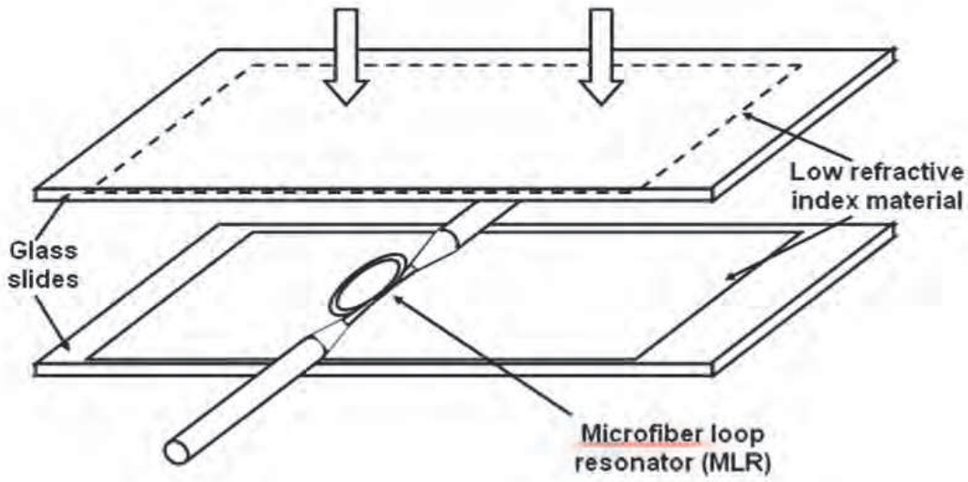

(a) diagram

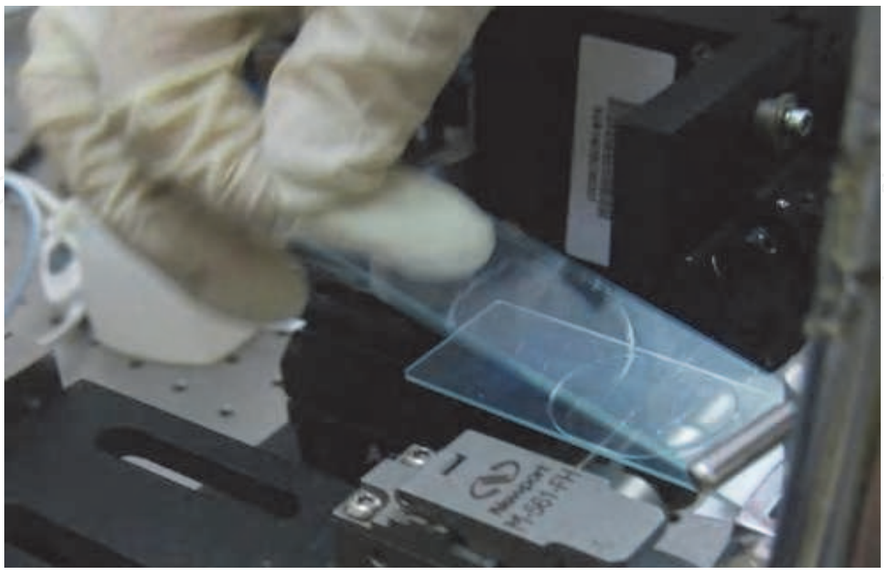

(b) Snapshot

Fig. 9. Packaging of the MLR (a) schematic diagram (b) snapshot

A MLR has a comb transmission spectrum similar to that of a Fabry–Perot filter. The resonant wavelength must satisfies $\lambda_m = 2\pi R n_{\text{eff}}/m$, where R is the radius of the ring, n_{eff} is the effective index of the ring, m is the resonant mode number. The resonant frequency spacing, i.e. Free Spectral Range (FSR), is given by [Sumetsky et al., 2006];

$$\Delta\nu_{FSR} = \frac{c}{2\pi R n_{eff}} \tag{3}$$

where c is the velocity of light in vacuum. The quality factor of a ring resonator can be expressed as

$$Q = \frac{\lambda_m}{\Delta\lambda_{\text{FWHM}}} \tag{4}$$

where $\Delta\lambda_{FWHM}$ is the 3 dB bandwidth of the resonant peak. The lower the coupling coefficient between the ring and straight waveguide, the higher the Q is. If the radius and the coupling coefficient of the ring are chose properly, the desired resonant frequency spacing and bandwidth of the resonant peak can be obtained. The measured comb transmission spectrum of the MLR is shown in Fig. 10, which was obtained by using the ASE source in conjunction with OSA. The resonant response of the MLR is obvious. The extinction ratio is about 4.0 dB, and the FSR is 0.08 nm.

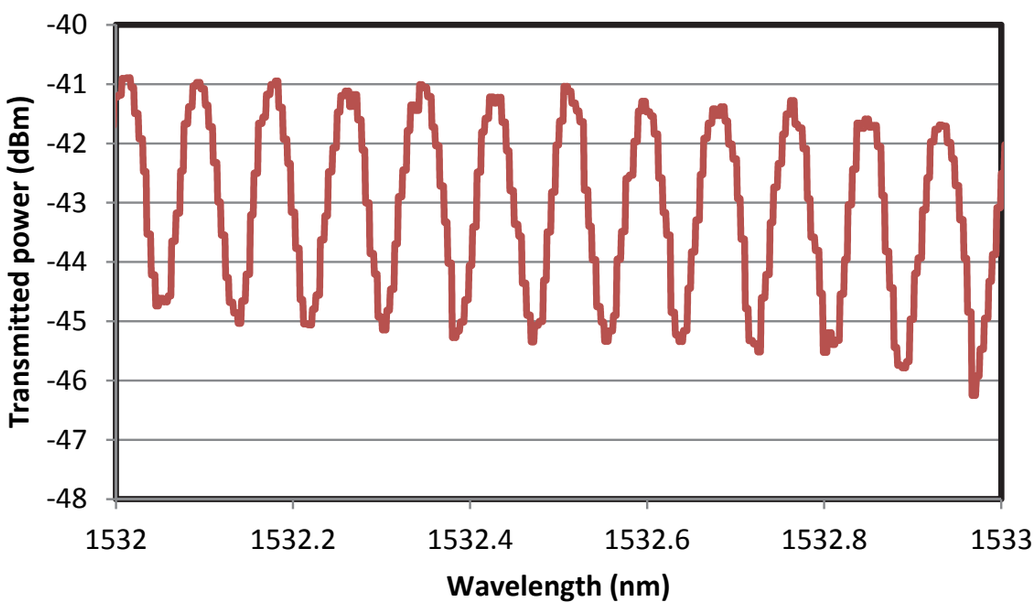

Fig. 10. Transmission spectrum of the fabricated MLR

The temperature response of the packaged MLR is then investigated. Fig. 11 shows the transmission spectrum of another packaged MLR at various temperatures. As shown in this figure, the spacing of the transmission comb spectrum is unchanged with the temperature. However, we observed a linear dependence of the extinction ratio of the MLR on temperature; higher temperature MLRs had a smaller extinction ratio. Fig. 12 shows an

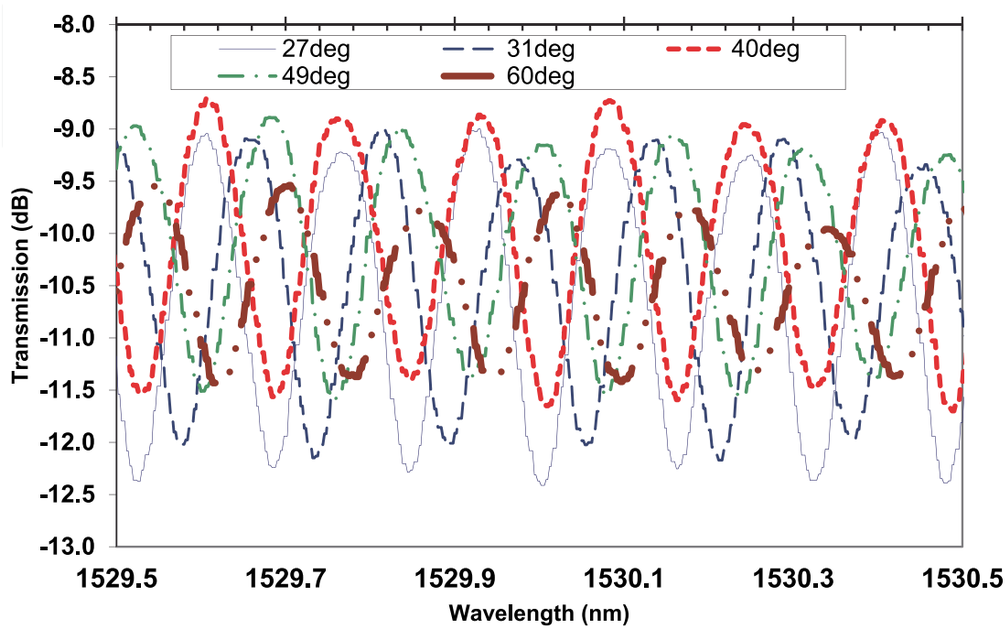

Fig. 11. Transmission spectra of the fabricated MLR obtained at various temperatures

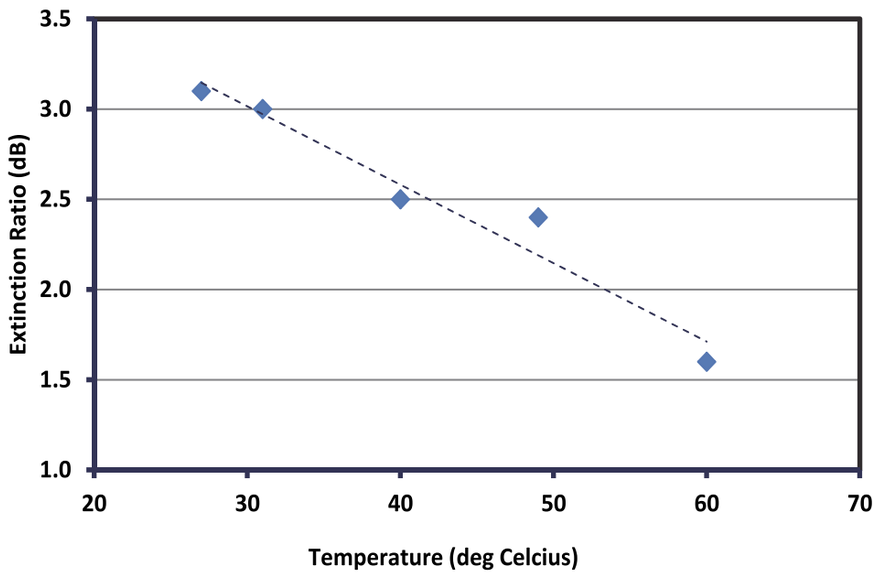

Fig. 12. Extinction ratio of the MLR as a function of the temperature

extinction ratio against the temperature. As seen, the slope of the extinction ratio reduction against temperature was about 0.043dB/^{o}C. The dependence of the extinction ratio on temperature is due to the change in the material's refractive index, which increase the loss at higher temperature and thus reduces the extinction ratio. In the proposed sensor, the optical path length is not much changed with the temperature and therefore, the comb spacing is unchanged as shown in Fig. 11.

5. Stimulated Brillouin scattering based temperature sensor

Brillouin scattering is an effect caused by the nonlinearity of a medium, whereby an incident pump photon can be converted into a scattered photon of slightly lower energy, usually propagating in the backward direction, and a phonon. At high optical pump powers, the Stimulated Brillouin scattering (SBS) is one of the most important nonlinear effects in fibers and has a significant influence on the operation of optical transmission systems as well as fiber sensors. Brillouin-based optical fiber sensors have been widely reported in recent years owing to their possibilities to perform distributed strain and temperature sensing along an optical fiber [Bao et al., 1993; Nikles et al., 1996; Culverhouse et al., 2008; Kee et al., 2002; Rathod et al., 1994]. Several techniques have been proposed for effective sensing using either spontaneous Brillouin scattering (SpBS) or stimulated Brillouin scattering (SBS) effects. Brillouin reflectometers are the most widely exploited in Brillouin-based optical sensing due to their simplicity. They are implemented by injecting a light beam into one of the sensing fibers' ends and are not affected by nonlocal effect, thus appearing more suitable for long range sensing applications. However, these type of sensors suffer from a small amplitude of the signal due to the use of spontaneous Brillouin scattering.

The configuration of the proposed sensor is shown in Fig. 13. It consists of a Brillouin pump (BP), an Erbium-doped fiber amplifier (EDFA), a ring cavity Brillouin gain block and a frequency shift measurement setup. The gain block consists of a piece of sensing fiber and a 3 dB coupler, which the Brillouin gain oscillates in an anti-clockwise direction to generate a BFL. The sensing fiber is located in an oven with temperature control and is shown in the dashed square in Fig. 13. An external cavity tunable laser source (TLS) with a line-width of approximately 20MHz is used as the BP. The BP light operating at 1555 nm is split into reference and probe signals, by using a 10dB coupler. The probe signal from 10% part is optically amplified by an EDFA to provide sufficient power for this study. This amplified signal is launched into a piece of sensing fiber through an optical circulator, which is also used to couple into the photodiode the backward propagating light from the ring cavity, including a BFL operating at wavelength downshifted by 0.08 nm from the BP wavelength. The output Brillouin signal is combined with the reference or BP signal by a 3 dB coupler for Brillouin shift measurement using a heterodyne technique. The combined optical signal is converted into an electrical signal by a phodiode which is connected to an RF spectrum analyzer.

To compare the performance achieved by various sensing fibers, a standard single-mode fiber (SMF), non-zero dispersion shifted fiber (NZ-DSF) and photonic crystal fiber (PCF) are alternatively employed as a gain medium in the BFL. The lengths of SMF, NZ-DSF and PCF are fixed at 25 km, 10 km and 100 m, respectively. The NZ-DSF has a core diameter of 4.2 μm and cut-off wavelength of 1150nm. The PCF has a triangular core with average diameter of 2.1 ± 0.3 μm and cladding diameter of 128 ± 5 μm. The average air hole diameter of the

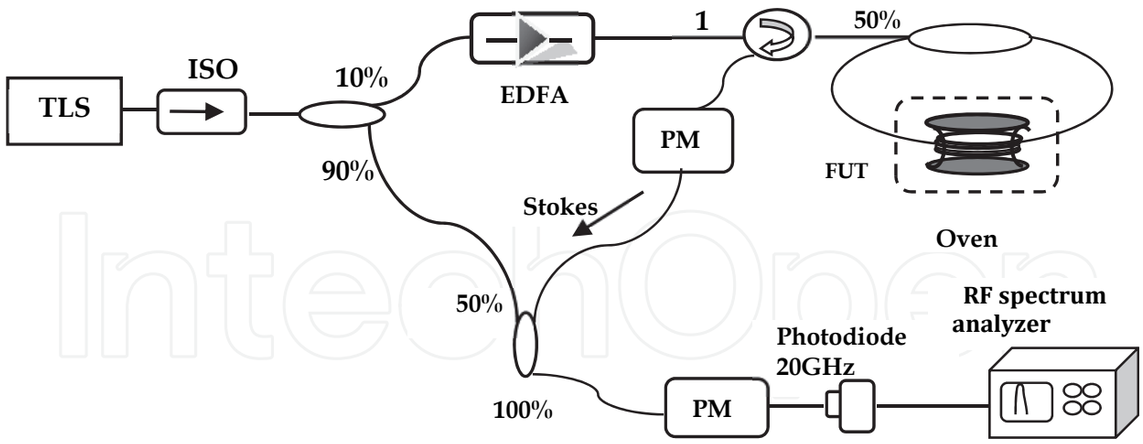

Fig. 13. Experimental setup for the spontaneous Brillouin scattering measurements.

fiber is 0.8 μm with 1.5 μm pitch. The PCF is made from pure silica with 17.4 wt% of Ge-doped core region. The SMF and NZ-DSF have core diameters of 9 and 4.2 μm, respectively. The sensing fiber is incorporated in a ring BFL configuration to reduce the required BP power for the operation. The Brillouin threshold is relatively lower for the SBS.

Fig. 14 shows the backward propagating Brillouin spectrum obtained from the ring cavity BFL, which is measured after the optical circulator by an OSA with resolution of 0.015 nm. In this experiment, the sensing fiber is NZ-DSF and the temperature is varied from 25oC to 80oC. The Brillouin Stokes laser is generated from interactions between the optical mode and acoustic modes in the fiber core. Thermally excited acoustic waves (acoustic phonons) produce a periodic modulation of the refractive index. Brillouin scattering occurs when light is diffracted backward on this moving grating, giving rise to frequency shifted Stokes and anti-Stokes components. This process can be stimulated when the interferences of the laser light and the Stokes wave reinforce the acoustic wave through electrostriction. Since the scattered light undergoes a Doppler frequency shift, the Brillouin shift depends on the acoustic velocity and is given by [Alahbabi et al., 2005]

$$\upsilon_B = \frac{2nV_a}{\lambda} \tag{5}$$

where V_a is the acoustic velocity within the fiber, n is the refractive index and λ is the vacuum wavelength of the incident lightwave. As shown in Fig. 14, the Brillluin Stokes is slightly shifted to a longer wavelength as the temperature is increased from 25°C to 80°C. This is attributed to the refractive index of the sensing medium, which increases with the temperature. Fig. 14 shows the Brillouin shift for the BFL with NZ-DSF, measured by the RF spectrum analyzer at two different temperatures; 25°C and 80°C. As shown in the figure, the Brillouin shift peak power shifted toward a higher frequency with increasing temperature. For a sensing fiber of NZ-DSF, at room temperature of 25°C, a value for υ_B is experimentally obtained at 10.7 GHz at 1550 nm wavelength region as shown in Fig. 15.

The strong attenuation of sound waves in silica determines the shape of the Brillouin gain spectrum. Actually, the exponential decay of the acoustic waves results in a gain presenting a Lorenzian spectral profile [Xiao-qiang et al., 2009].

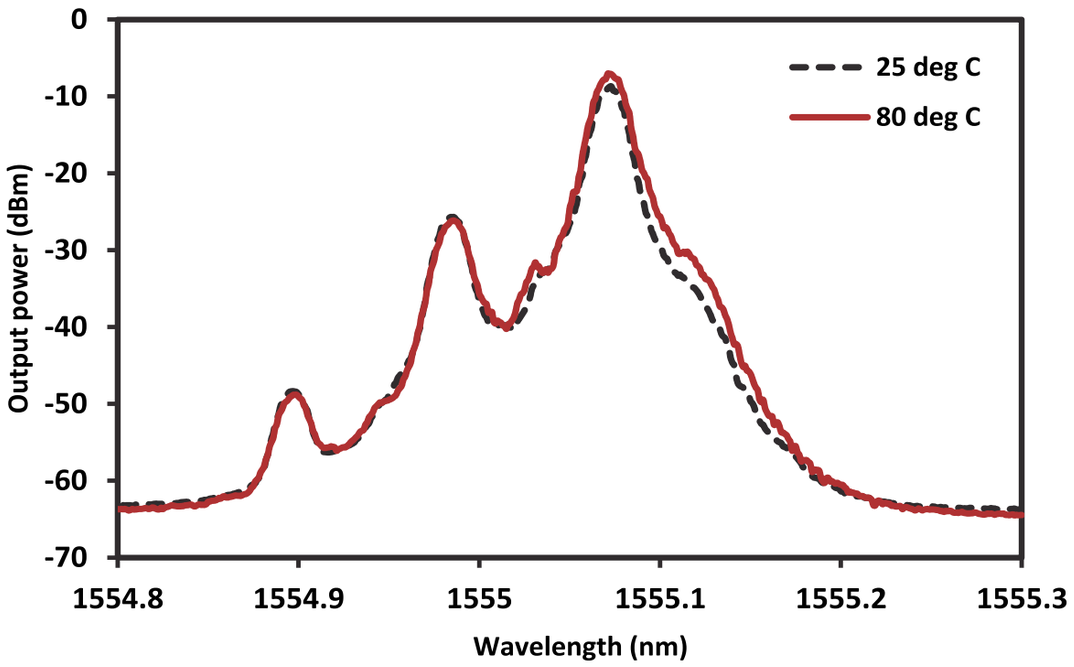

Fig. 14. Stimulated Brillouin scattering monitored by OSA in minimum and maximum used temperature.

$$g_B(\upsilon) = g_0 \frac{(\Delta\upsilon_B/2)^2}{(\upsilon-\upsilon_B)^2 + (\Delta\upsilon_B/2)^2} \tag{6}$$

where ΔvB is the full-width at half maximum (FWHM). The Brillouin gain spectrum peaks at the Brillouin frequency shift v_B (or the frequency difference between the two beams), and the peak value is given by the Brillouin gain coefficient

$$g_B(\upsilon) = g_0 = \frac{2\pi n^7 p_{12}^2}{c\lambda_p^2 \rho_0 V_a \Delta\upsilon_B} \tag{7}$$

where p_{12} is the longitudinal elasto-optic coefficient, ρ_0 is the density, λ_p is the pump wavelength and c is the vacuum velocity of light [Heiman et al., 1979; Agrawal, 1989]. The Brillouin linewidth for a spontaneous Brillouin scattering in a standard SMF is reported to be approximately 30 MHz, which can be calculated using Eq. (7). In this work, the Brillouin linewidth is observed to be around 15 MHz as shown in Fig. 13 due to the proposed sensor, which is based on SBS effect. The Brillouin linewidth is also expected to slightly increases with the temperature increase.

The temperature–dependence of the Brillouin gain shift is also investigated for various types of sensing fibers and the result is shown in Fig. 16. The beat frequency is obtained at approximately 10.85, 10.75 and 9.80 GHz with the sensing fibers of SMF, NZ-DSF and PCF, respectively. It is also observed that the central frequency linearly increases with the temperature over a wide temperature range. The slope coefficients of 0.77, 0.56 and 1.45 MHz/oC are obtained for BFLs using SMF, NZ-DSF and PCF, respectively. The error bars

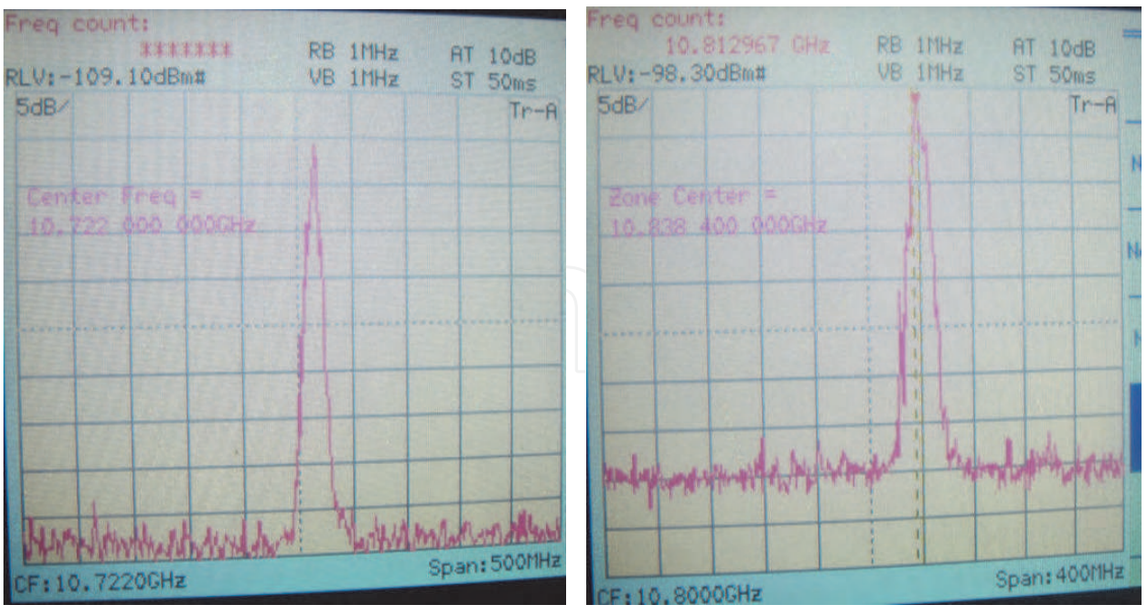

Fig. 15. The typical SBS beat frequency spectra at the minimum and maximum temperatures using the NZ-DSF as the sensing fiber.

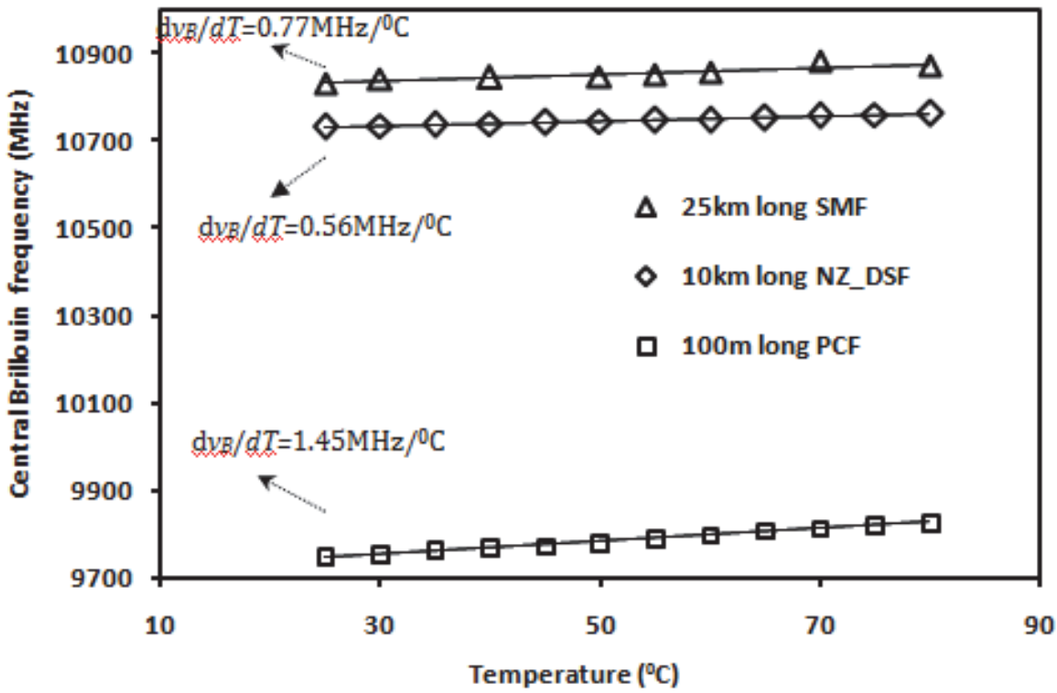

Fig. 16. Brillouin frequency shift as functions of temperature.

are ±3 MHz, corresponding to the BFS fluctuations when the temperature is fixed. All fiber samples are only coated with a thin acrylate micro jacket, so that the coating influence is expected to be kept below 0.1 MHz/ oC. This experiment indicates that the PCF with small core is preferable for this application. As also shown in Fig. 16, the Brillouin shift for PCF is

less than that of the other silica fibers. The reason is due to the Germania concentration in the fiber core such that the inhomogeneous distribution within the core of the fiber is responsible for multi peaks in Brillouin gain spectrum. The PCF used is composed of a small-scale solid silica core comprising a Ge-doped center region with multiple air holes arranged in a hexagonal lattice around the core which act as cladding. With the combination of a large refractive index contrast between the silica core and the air-filled microstructure, the PCF can confine the mode tightly in the core that results in a low effective mode area and thereby produce a large nonlinear coefficient. This characteristic avoids the difficulty in distributed fiber sensors that use long SMF and NZ-DSF which contributes to uncertainty in the sensing results. Although the threshold is reduced by the increased length necessary to provide the SBS, it creates other problems like reduced coefficient for sensing temperature.

6. Conclucions

Four different approaches for temperature sensing have been demonstrated; intensity modulated FODS, lifetime measurements, MLR-based and SBS-based sensors. The first sensor uses a fiber-optic displacement sensor based on a multimode POF coupler to measure temperature ranging from 42^0C to 90^0C. The displacement curve has a sensitivity of 0.0005 mV/μm and a linearity of more than 99% within a measurement range between 0 to 1400 μm. By placing the aluminum rod within the linear range, the measured output signal is observed to be a linear function of the aluminum rod temperature with a sensitivity of 0.0044 mV/^{o}C for temperature detection with a linearity of more than 98% and a resolution of 2.4 ^{o}C. The second sensor is based on a lifetime measurement of 90 cm long of EDF, which is diode-pumped by a modulated 980 nm laser. The sensitivity of the sensor is obtained at 0.009 ms/^{o}C with a linearity of more than 94%. This temperature sensor is shown to be effective and useful for its high resolution and precision. The third sensor is based on MLR, which is fabricated from a microfiber, which is derived using a flame heating method. The MLR is constructed by coiling the microfiber to form a loop resonator device. The device is embedded into low refractive index polymer for robustness. The spacing of the transmission comb spectrum of the MLR is observed to be unchanged with the temperature. However, the extinction ratio of the spectrum is observed to be linearly decreasing with the temperature. The slope of the extinction ratio reduction against temperature was about 0.043dB/^{o}C. The dependence of the extinction ratio on temperature is due to the change in the material's refractive index. The temperature-dependence of the Brillouin frequency shift is demonstrated in various types of fiber in the last approach. The beat frequency between the SBS and pump signals is measured using the heterodyne method. The central Brillouin beat frequency increases linearly with increasing temperature with temperature coefficients of 0.77, 0.56 and 1.45MHz/^{0}C. The phenomena are demonstrated for 25 km long SMF, 10 km long NZ-DSF and 100 m PCF, respectively.

7. References

Alahbabi M N, Cho Y T, Newson T P. 150-km-range distributed temperature sensor based on coherent detection of spontaneous Brillouin backscatter and in-line Raman amplification. Journal of the Optical Society of America: B, 2005, 22(6): 1321–1324.

Bao X, Webb D J, Jackson D A. 32-km distributed temperature sensor using Brillouin loss in optical fiber. Optics Letters, 1993, 18(18): 1561–1563.

Choi, H. Y., K. S. Park, et al. (2008). "Miniature fiber-optic high temperature sensor based on a hybrid structured Fabry–Perot interferometer." Optics letters 33(21): 2455-2457.

Culverhouse, D., F. Farahi, et al. (2008). "Potential of stimulated Brillouin scattering as sensing mechanism for distributed temperature sensors." Electronics Letters 25(14): 913-915.

D. Heiman, D. S. Hamilton, and R. W. Hellwarth, "Brillouin scattering measurements on optical glasses," *Phys. Rev. B*, vol. 19, p. 6583, 1979.

F. Xu, V. Pruneri, V. Finazzi, and G. Brambilla, "High Sensitivity Refractometric Sensor Based on Embedded Optical Microfiber Loop Resonator," in Conference on Lasers and Electro-Optics/Quantum Electronics and Laser Science Conference and Photonic Applications Systems Technologies, OSA Technical Digest (CD) (2008), paper CMJ7.

Golnabi, H. (2000). "Simulation of interferometric sensors for pressure and temperature measurements." Review of scientific Instruments 71: 1608.

G. P. Agrawal, *Nonlinear Fiber Optics*. Boston, MA: Academic, 1989.

Guo, Q., M. Nishio, et al. (2003). "Temperature dependence of aluminum nitride reflectance spectra in vacuum ultraviolet region." Solid State Communications 126(11): 601-604.

H. Ahmad, W. Y. Chong, K. Thambiratnam, M. Z. Zulklifi, P. Poopalan, M. M. M. Thant and S. W. Harun, "High Sensitivity Fiber Bragg Grating Pressure Sensor Using Thin Metal Diaphragm," IEEE Sensors J., 9 (12), pp. 1654-1659, 2009.

H. C. Nguyen, B. T. Kuhlmey, E. C. Magi, M. J. Steel, P. Domachuk, C. L. Smith, and B. J. Eggleton, "Tapered photonic crystal fibers: Properties, characterization and applications," Appl. Phys. B, vol. 81, pp. 377–387, Jul. 2005.

H. C. Seat, J. H. Sharp, Z. Y. Zhang, K. T. V. Grattan, "Single-crystal ruby fiber temperature sensor," Sensors and Actuators A, Vol. 101, pp. 24-29, 2002.

H. Z. Yang, S. W. Harun and H. Ahmad, "Theoretical and experimental studies on concave mirror-based fiber optic displacement sensor," Sensor Review, Vol. 31, pp. 65-69 (2011).

J. Castrellon-Uribe, "Experimental results of the performance of a laser fiber as a remote sensor of temperature," Optics and Lasers in Engineering, Vol. 43, pp. 633-644, 2005.

J. Villatoro, V. P. Minkovich, and D. Monzón-Hernández, "Temperature independent strain sensor made from tapered holey optical fiber," Opt. Lett., vol. 31, pp. 305–307, Feb. 2006.

K. Amarnath, R. Grover, S. Kanakaraju, P. T. Ho, "Electrically pumped InGaAsP-InP microring optical amplifiers and lasers with surface passivation", IEEE Photon. Technol. Lett., vol. 17, pp. 2280-2282, 2005.

Kee, H. H., G. Lees, et al. (2002). "1.65 m Raman-based distributed temperature sensor." Electronics Letters 35(21): 1869-1871.

K. J. Han, Y. W. Lee, J. Kwon, S. Roh, J. Jung and B. Lee, "Simultaneous measurement of strain and temperature incorporating a long-period fiber grating inscribed on a polarization-maintaining fiber," IEEE Photon. Technol. Lett., Vol. 16, pp. 2114–2116, 2004.

K. S. Lim, S. W. Harun, H. Z. Yang, K. Dimyati and H. Ahmad, "Analytical and experimental studies on asymmetric bundle fiber displacement sensors," J. Modern Optics, 56 (17), pp. 1838-1842, 2009.

L. Li, X. Y. Dong, L. Y. Shao, C. L. Zhao and Y. L. Sun, "Temperature-independent acceleration measurement with a strain-chirped fiber Bragg grating," Optoelectronics and advanced materials – rapid communications, Vol. 4, No. 7, pp. 943-946, 2010.

L. Tong, L. Hu, J. Zhang, J. Qiu, Q. Yang, J. Lou, Y. Shen, J. He, Z. Ye, "Photonic nanowires directly drawn from bulk glasses," Opt. Express, Vol. 14 (1) pp. 82-87, (2006).

M. McSherry, C. Fitzpatrick and E. Lewis, "Review of luminescent based fibre optic temperature sensors," Sensor Review, Vol. 25, pp. 56-62, 2005.

M. Sumetsky, Y. Dulashko, J. M. Fini, A. Hale, and D. J. DiGiovanni, "The Microfiber Loop Resonator: Theory, Experiment, and Application," J. Lightwave Technol. Vol. 24, No. 1, 2006, pp. 242-250.

M. Yasin, S. W. Harun, H. Z. Yang and H. Ahmad, "Title: Fiber optic displacement sensor for measurement of glucose concentration in distilled water," Optoelectronics and advanced materials – rapid communications, Vol. 4, No. 8, pp. 1063-1065, 2010.

M. Yasin, S.W. Harun, W.A. Fawzi, Kusminarto, Karyono, H. Ahmad., "Lateral and axial displacements measurement using fiber optic sensor based on beam-through technique", Microwave And Optical Technology Letters, Vol. 51, pp. 2038-2040 (2009).

Nikles M, Thevenaz L, Robert P. Simple distributed fiber sensor based on Brillouin gain spectrum analysis. Optics Letters, 1996, 21(10): 758–760.

R. Rathod, R. D. Pechstedt, D. A. Jackson, D. J. Webb, "Distributed temperature-change sensor based on Rayleigh backscattering in an optical fiber," Opt. Lett., Vol. 19, pp. 593–595, 1994.

S. Baek, Y. Jeong, J. Nilson, J. K. Sahu, B. Lee, "Temperature-dependent fluorescence characteristics of an ytterbium-sensitized erbium-doped silica fiber for sensor applications," Optical Fiber Technology, Vol. 12, pp. 10-19, 2006.

SUN Xiao-qiang, XU Kun, PEI Yin-qing, FUSong-nian, "Simple distributed optical fiber sensor based on Brillouin amplification of microwave photonic signal" The journal of China Universities of Posts and telecommunications, 2009, 16: 24-28.

S. W. Harun, K. S. Lim, A. A. Jasim, H. Ahmad, "Dual wavelength erbium-doped fiber laser using a tapered fiber, Journal of Modern Optics, Vol. 57, pp. 1362-3044 (2010).

V. Lopez, G. Paez and M. Strojnik, "Sensitivity of a temperature sensor, employing ratio of fluorescence power in a band," Infrared Physics & Technology, Vol. 46, pp. 133–139, 2004.

V. P. Minkovich, J. Villatoro, D. Monzón-Hernández, S. Calixto, A. B. Sotsky, and L. I. Sotskaya, "Holey fiber tapers with resonance transmission for high-resolution refractive index sensing," Opt. Express, vol. 13, pp. 7609–7614, Sep. 2005.

Van Etten, W. and J. Van der Plaats (1991). Fundamentals of optical fiber communications.

Vijay K. Kulkarni, Anandkumar S. Lalasangi, I. I. Pattanashetti, U. S. Raikar, "Fiber Optic Micro-Displacement Sensor Using Coupler," Journal Of Optoelectronics And Advanced Materials Vol. 8, No. 4, August 2006, P. 1610 – 1612

X. Jiang, L. Tong, G. Vienne, X. Guo, A. Tsau, Q. Yang and D. Yang, "Demonstration of optical microfiber knot resonators," Appl. Phys. Lett., Vol. 88 (22), pp. 223501 (2006)

X. Jiang, Q. Yang, G. Vienne, Y. Li, L. Tong, Demonstration of microfiber knot laser Appl. Phys. Lett. 89 (14) (2006) 143513.

Y. Li, L. Tong, Opt. Lett. 33 (4) (2008) 303.

Y. Lou, L. M. Tong, and Z. Z. Ye, "Modeling of silica nanowires for optical sensing," Opt. Express, vol. 13, pp. 2135-2140 (2005)

Zhang, Z., K. Grattan, et al. (2009). "Fiber optic high temperature sensor based on the fluorescence lifetime of alexandrite." Review of scientific Instruments 63(8): 3869-3873.

Optical Fiber Communications and Devices

Edited by Dr Moh. Yasin

ISBN 978-953-307-954-7
Hard cover, 380 pages
Publisher InTech
Published online 01, February, 2012
Published in print edition February, 2012

This book is a collection of works dealing with the important technologies and mathematical concepts behind today's optical fiber communications and devices. It features 17 selected topics such as architecture and topologies of optical networks, secure optical communication, PONs, LANs, and WANs and thus provides an overall view of current research trends and technology on these topics. The book compiles worldwide contributions from many prominent universities and research centers, bringing together leading academics and scientists in the field of photonics and optical communications. This compendium is an invaluable reference edited by three scientists with a wide knowledge of the field and the community. Researchers and practitioners working in photonics and optical communications will find this book a valuable resource.

How to reference

In order to correctly reference this scholarly work, feel free to copy and paste the following:

S. W. Harun, M. Yasin, H. A. Rahman, H. Arof and H. Ahmad (2012). Fiber Optic Temperature Sensors, Optical Fiber Communications and Devices, Dr Moh. Yasin (Ed.), ISBN: 978-953-307-954-7, InTech, Available from: http://www.intechopen.com/books/optical-fiber-communications-and-devices/fiber-optic-temperature-sensors

INTECH
open science | open minds

InTech Europe
University Campus STeP Ri
Slavka Krautzeka 83/A
51000 Rijeka, Croatia
Phone: +385 (51) 770 447
Fax: +385 (51) 686 166
www.intechopen.com

InTech China
Unit 405, Office Block, Hotel Equatorial Shanghai
No.65, Yan An Road (West), Shanghai, 200040, China
中国上海市延安西路65号上海国际贵都大饭店办公楼405单元
Phone: +86-21-62489820
Fax: +86-21-62489821

IntechOpen